

The Non-Axisymmetric Influence: Radius and Angle-Dependent Trends in a Barred Galaxy

Carrie Filion,¹★ Rachel L. McClure,² Martin D. Weinberg,³ Elena D’Onghia,² Kathryne J. Daniel⁴

¹William H. Miller III Department of Physics & Astronomy, The Johns Hopkins University, Baltimore, MD 21218

²Department of Astronomy, University of Wisconsin–Madison, Madison, WI, 53706

³Department of Astronomy, University of Massachusetts at Amherst, Amherst, MA 01003, USA

⁴Department of Astronomy & Steward Observatory, University of Arizona, Tucson, AZ, 85721

arXiv:2302.01307v1 [astro-ph.GA] 2 Feb 2023

Accepted XXX. Received YYY; in original form ZZZ

ABSTRACT

Many disc galaxies host galactic bars, which exert time-dependent, non-axisymmetric forces that can alter the orbits of stars. There should be both angle and radius-dependence in the resulting radial re-arrangement of stars (‘radial mixing’) due to a bar; we present here novel results and trends through analysis of the joint impact of these factors. We use an N-body simulation to investigate the changes in the radial locations of star particles in a disc after a bar forms by quantifying the change in orbital radii in a series of annuli at different times post bar-formation. We find that the bar induces both azimuth angle- and radius-dependent trends in the median distance that stars have travelled to enter a given annulus. Angle-dependent trends are present at all radii we consider, and the radius-dependent trends roughly divide the disc into three ‘zones’. In the inner zone, stars generally originated at larger radii and their orbits evolved inwards. Stars in the outer zone likely originated at smaller radii and their orbits evolved outwards. In the intermediate zone, there is no net inwards or outwards evolution of orbits. We adopt a simple radius-dependent initial metallicity gradient and discuss recent observational evidence for angle-dependent stellar metallicity variations in the Milky Way in the context of this toy model. We briefly comment on the possibility of using observed angle-dependent metallicity trends to learn about the initial metallicity gradient(s) and the radial re-arrangement that occurred in the disc.

Key words: galaxies: evolution – galaxies: kinematics and dynamics – galaxies: bar – galaxies: disc

1 INTRODUCTION

In the past half-century, significant effort has gone into defining and understanding the dynamical processes through which stars in disc galaxies can move away from their birth radii. A wide variety of dynamical processes have been proposed and explored, each with varying degrees of clear applicability in the Milky Way. The Milky Way is host to a variety of structures that cause time-dependent gravitational forces and drive long-term orbital evolution. In this analysis, we examine effects from one of the strongest perturbations in the Milky Way – the Galactic bar (see e.g. Blitz & Spergel 1991, Weinberg 1992).

Standard Hamiltonian perturbation theory predicts that a central bar can radially redistribute disc orbits (e.g. Binney & Tremaine 2008), changing both the radial and angular distribution of stars. In a disc with a radius-dependent initial metallicity gradient, azimuth angle-dependent metallicity variations would be an observational result of these radial changes. It is in this context that trends in angle dependence in disc galaxies are typically explored (e.g. Di Matteo et al. 2013, see also the test particle simulation presented in Wheeler et al. 2022 and the more spiral-focused analyses of Grand et al. 2016, Khoperskov et al. 2018, Fragkoudi et al. 2018).

Azimuthal metallicity variations can also be induced from external perturbations. Angle-dependent metallicity variations have been

observed in the gas phase of close galaxy pairs with integral field unit spectroscopy (Hwang et al. 2019), and are predicted to arise in stellar populations from galactic mergers (e.g. the Sagittarius-like merger presented in Carr et al. 2022). In the Milky Way, it is likely that both internal non-axisymmetric structures (such as the bar) and external perturbations (such as Sagittarius) are altering the orbits of stars in the disc. It is important to understand the role of each, and in this analysis we focus on the radius and angle-dependent trends that can arise from a bar alone.

The formation and evolution of a bar alters the orbits of stars in a disc galaxy in a few key ways. The first is the exchange of angular momentum between stars and the bar as the bar is forming and growing. The bar ‘steals’ angular momentum from stars in the bar region and transports angular momentum outwards (see e.g. Lynden-Bell & Kalnajs 1972, and more recent discussion in Petersen et al. 2019). The second is through resonant interactions and the bar exerting torques on the stars in the disc, altering the stars’ orbital properties. Finally, the existence of a strong non-axisymmetric potential from the bar modifies the radial distribution of stars.

Unlike many of the earlier analyses discussed above, we perform our dynamical analysis in terms of ‘present-day’ and initial (or ‘birth’) radii, not metallicity, and we tag the initial radius of the stars as their radial location at the time that the bar has reached its maximum amplitude. Framing the analysis in terms of radii (instead of metallicity) allows us to more easily explore how the dynamics from a bar and its evolution alters the orbits of stars within the disc,

★ E-mail: cfilion@jhu.edu

and what angle- and radius-dependent signature this evolution leaves on the stars in a given annulus.

Further, many studies define the initial (or ‘birth’) radial position of a star to correspond to its location at some time before the bar forms and then perform their analysis at time(s) post bar-formation. We instead define our initial radial position to correspond to a time *after* the bar has formed. We do this to isolate the effects of bar evolution on the disc, separating these effects from those of the bar formation process. As such, this analysis focuses on ‘younger’ to ‘intermediate age’ stars (~ 1 to 4 Gyr), whereas studies such as [Di Matteo et al. \(2013\)](#) investigate ‘ancient’ stars.

We opt to explore the signatures of bar-driven evolution within annuli at discrete times post bar-formation, such that we can investigate the amplitude of the angle-dependent radial re-arrangement as a function of both radial position and time. We make no restrictions on orbital circularity and explore the changes in the (instantaneous) orbital radii of a stars that are the end result of bar-induced dynamical processes. The term ‘radial mixing’ is occasionally defined to describe any radial change, but to avoid any possible confusion with alternate connotations we explicitly avoid using this term.

We provide the details of our N-body simulation in Section 2. In Section 3 we present the results of our investigation of the radial distances that stars have traversed in terms of the initial and present-day Galactocentric cylindrical radii (R) of the stars. We then adopt a simple initial metallicity gradient and discuss angle-dependent metallicity variations in the context of this toy model in Section 4. We discuss broader implications of our dynamical results in Section 5 and conclude in Section 6.

2 METHODS

2.1 Simulations

We use a self-consistent, collisionless N-body simulation of an isolated, barred galaxy, which was evolved using the basis function expansion code EXP ([Weinberg 1999](#), see [Petersen et al. 2022](#) for a recent description). The initial conditions for this galaxy are nearly identical to the model presented in Table 1 of [Petersen et al. \(2021\)](#) as ‘Potential I’, and we highlight below where the models differ. We provide the key parameters of the simulation here, and refer to [Petersen et al. \(2021\)](#) for in-depth discussion of the simulation and its initial conditions. Note that this simulation is in virial units (where $R_{vir} = G = M_{vir} = t_{vir} = 1$) and we scale to physical units with the following scaling, chosen to roughly approximate the Milky Way: $R_{vir} = 300$ kpc, $M_{vir} = 1.4 \times 10^{12} M_\odot$, and $t_{vir} = 2$ Gyr.

The galaxy consists of a live dark matter halo of $N_d = 10^7$ particles and a disc of $N_s = 10^6$ particles. The dark matter halo is a modified Navarro-Frenk-White potential ([Navarro et al. 1997](#)) that matches the distribution function given for ‘Potential I’ in [Petersen et al. \(2021\)](#). For this analysis, however, we have set the ‘concentration parameter’ to equal 20 (instead of 25, as was adopted for ‘Potential I’) to better match the combined disc and halo rotation curve of the Milky Way (M. Petersen, *priv. comm.*).

The stellar disc of the galaxy has an exponential density distribution in radius and an isothermal-sech² distribution in height. The disc mass is equal to $0.025M_{vir}$, the scale length (R_d) is $R_d = 0.01R_{vir} \sim 3$ kpc, and the scale height (z_0 , constant throughout the disc) is $z_0 = 0.001R_{vir} \sim 300$ pc. The initial value of the Toomre Q parameter (set by the surface density of the disc, the epicyclic frequency, and the radial velocity dispersion) is ≈ 1.4 .

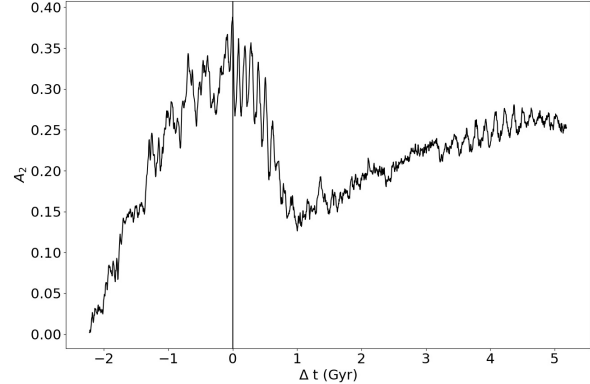


Figure 1. The strength of the bar over time, measured within a galactocentric cylindrical annulus between 0.75 to 1.5 kpc. Here, time is given as $\Delta t = t - t_0$, where t_0 corresponds to the time where the bar strength is at maximum (also shown as vertical black line).

2.2 Bar Properties

Structure forms naturally in the disc relatively quickly in the simulation. A strong bar is evident, as well as weaker trailing $m = 2$ arms outside of the bar-dominated region. We compute both the bar strength and length using the relative amplitude of the $m = 2$ Fourier components of the face-on disc, using the following expression,

$$A_2 = \frac{|\sum_j M_j e^{2i\phi_j}|}{\sum_j M_j}, \quad (1)$$

where M_j is the mass of the j^{th} particle and ϕ_j is its galactocentric azimuthal (ϕ) coordinate location (see e.g. [Sellwood & Athanassoula 1986](#), [D’Onghia & L. Aguerri 2020](#), [Baba et al. 2022](#)). In computing the bar strength, we compute A_2 within a portion of the bar region. Specifically, the summation is performed over all stars within a Galactocentric cylindrical annulus between 0.75 to 1.5 kpc at each time step.

We define the time at which the bar has finished forming (hereafter initial time, $t = t_0$) to be when the bar strength reaches its maximum. We present a plot of bar strength over time in Figure 1, where the vertical line indicates $t = t_0$. We analyse the galaxy’s angular trends at one, two, three, and four gigayear after t_0 (where a gigayear corresponds to roughly three and a half bar rotations as determined by the bar pattern at $t = t_0$).

In computing the bar length (R_{bar}), the summation is done over the stars that reside in annular rings of width 0.1 kpc from $R = 0.3$ kpc to $R = 15$ kpc at a given timestep. We identify the maximum of the relative amplitude of the $m = 2$ feature at each time step, and then estimate the length of the bar to be where the relative amplitude drops to $\sim 20\%$ of this maximum value (such that this radius is larger than that where the amplitude is maximum), following e.g. [Athanassoula & Misiriotis \(2002\)](#). We adopt this specific metric as it enables direct comparison to the Milky Way bar, whose length has been estimated in the same way (see e.g. [Wegg et al. 2015](#)), but note that it is susceptible to over-estimation due to trailing $m = 2$ structure.

Finally, following Appendix B.3 of [Petersen et al. \(2021\)](#), we compute the approximate location of corotation with the bar (R_{CR}) as the radius where the circular frequency and the pattern speed are

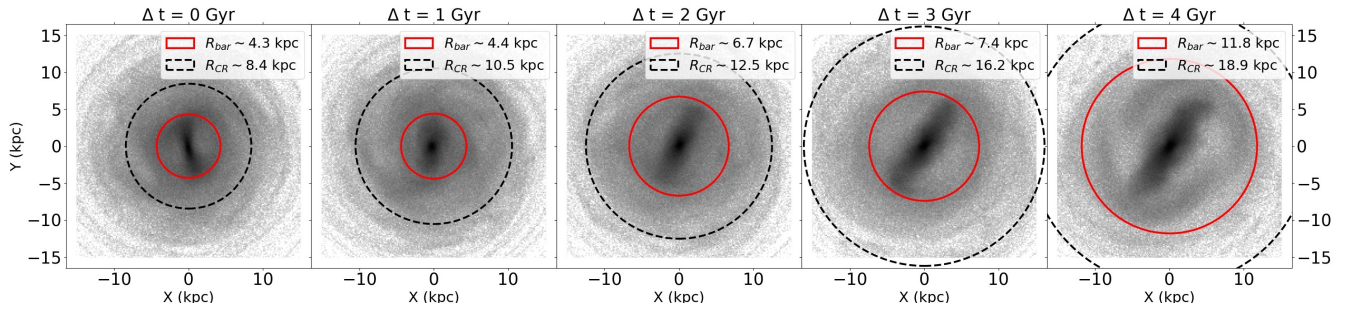


Figure 2. The face-on view of the galaxy at $\Delta t = 0, 1, 2, 3$, and 4 gigayear. The colour indicates log-scaled density, with darker grey indicating regions of higher density. Red and black circles indicate the approximate length of the bar and the location of corotation, respectively. Here, corotation is estimated as the radius where the circular frequency and pattern speed are equal. The disc rotates counter-clockwise.

equal¹. We present the face-on density plots of the galaxy at each of the selected time steps in Figure 2, where the approximate length of the bar and corotation radii are indicated with a red and black circle, respectively.

2.3 Dynamical Analysis

We select twelve annuli centered on $R = 1$ through 12 kpc, each of width of 0.5 kpc (i.e. ± 0.25 kpc). We investigate the median radial distance that stars in a given annulus traversed to get to their present location as a function of azimuth angle. We refer to this median, angle-dependent radial distance as ΔR . We use the observable *instantaneous* galactocentric cylindrical radius (as opposed to e.g. guiding center radii).

To compute ΔR , we first compute the change in galactocentric radius (δR , where $\delta R = R_t - R_{t_0}$, where R_{t_0} is the initial or ‘birth’ radius, and negative δR indicates that the star originated at a larger radius than the present location) for each of the stars that are in a given annulus at each time interval. We divide each annulus into 4° -wide azimuth bins, and ΔR for each bin is then the median value of δR of that bin.

We refer to this angle-dependent median distance in a given annulus (ΔR) as the ‘bulk’ radial change happening in the disc. The bulk trends that we discuss in this analysis cannot describe all of the radial changes happening in a galaxy, as any given star could travel more or less than the median distance. We leave more thorough analysis of individual dynamical families of stars and the mechanisms causing their radial changes to future study (Filion et al, in prep).

3 RESULTS

Here, we detail the bulk radial changes that occur in the disc. We restrict this Section to the results of the dynamical analysis, and in Section 4, we make connections to potentially observable signatures.

3.1 Trends in the Bulk Radial Changes

In Figure 3 we present ΔR as a function of ϕ for all of the annuli at each time interval. For clarity, we include four annuli per column. In

¹ Note that the weak bar assumption of near-circular orbits on which such definitions of corotation are based begins to break down in the presence of strong non-axisymmetric forces, such as the bar in this galaxy. It is for this reason that we limit the extent to which we make use of this estimate.

each plot, the vertical lines indicate the angle of the bar (measured relative to the positive x-axis) at that time. Angle-dependent, sinusoidal variations in ΔR are seen clearly in most annuli at all times, with the larger radii generally becoming more sinusoidal in time. The strength of alignment of the variations with the bar angle depends on the length of the bar relative to the chosen annulus. Annuli within the extent of the bar are well-aligned with the bar, while those further outside of the bar lag and can be up to ~ 1 radian offset from the bar. In Table 1, we provide the maximum and minimum values of ΔR in each annulus computed in the angular bins given above, alongside the angle-averaged mean ΔR (i.e. $\langle \Delta R \rangle_\phi$) values. The maximum and minimum columns provide insight into the angle-dependent variations, while the mean column provides information on the angle-averaged radial rearrangement occurring in the disc.

We present an alternative view of these angle-dependent variations in Figure 4, which shows face-on two-dimensional histograms of the annuli at each time colour-coded by the mean δR in ~ 0.1 kpc-wide hexagonal bins. Here, density contours of the disc are over plotted in black. The face-on view of the angle-dependent trends are quadrupole-like, and the combination of Figure 3 and 4 reveal that the quadrupole becomes more coherent over time as the bar grows to encompass more of the disc. We note that in each of these plots, we have included all stars in a given annulus regardless of height above the plane, but the results are essentially identical if we restrict the discussion to stars near the plane (e.g. $|z| < 0.3$ kpc, or one disc scale height).

3.2 Implications

At all times, the innermost annuli (left column of Figure 3, where $R \lesssim R_d$ and $R \lesssim R_{\text{bar}_0}$, with $R_{\text{bar}_0} \sim 4.3$ kpc being the length of the bar at $\Delta t = 0$ Gyr) orbits have evolved inwards and there is a median negative change. The intermediate annuli (middle column, $R \gtrsim R_d$ and $R \gtrsim R_{\text{bar}_0}$) are composed of a mix of stars whose orbits have evolved inward and outward, with the outward evolving regions generally aligned with the bar major axis, and inward evolving regions generally aligned with the minor axis. Annuli at radii larger than the bar length are less well-aligned with the bar than those within the bar edge. This worsening alignment is due to the transition to trailing, spiral structure (also an $m = 2$ feature) outside of the bar-dominated region. The outer annuli (right column, $R \gg R_d$ and $R > R_{\text{bar}_0}$) are skewed such that there is a positive median change and orbits have evolved outwards, especially at late times.

The combination of this bulk inward (and outward) evolution with azimuth angle-dependence has not been explicitly explored as far as

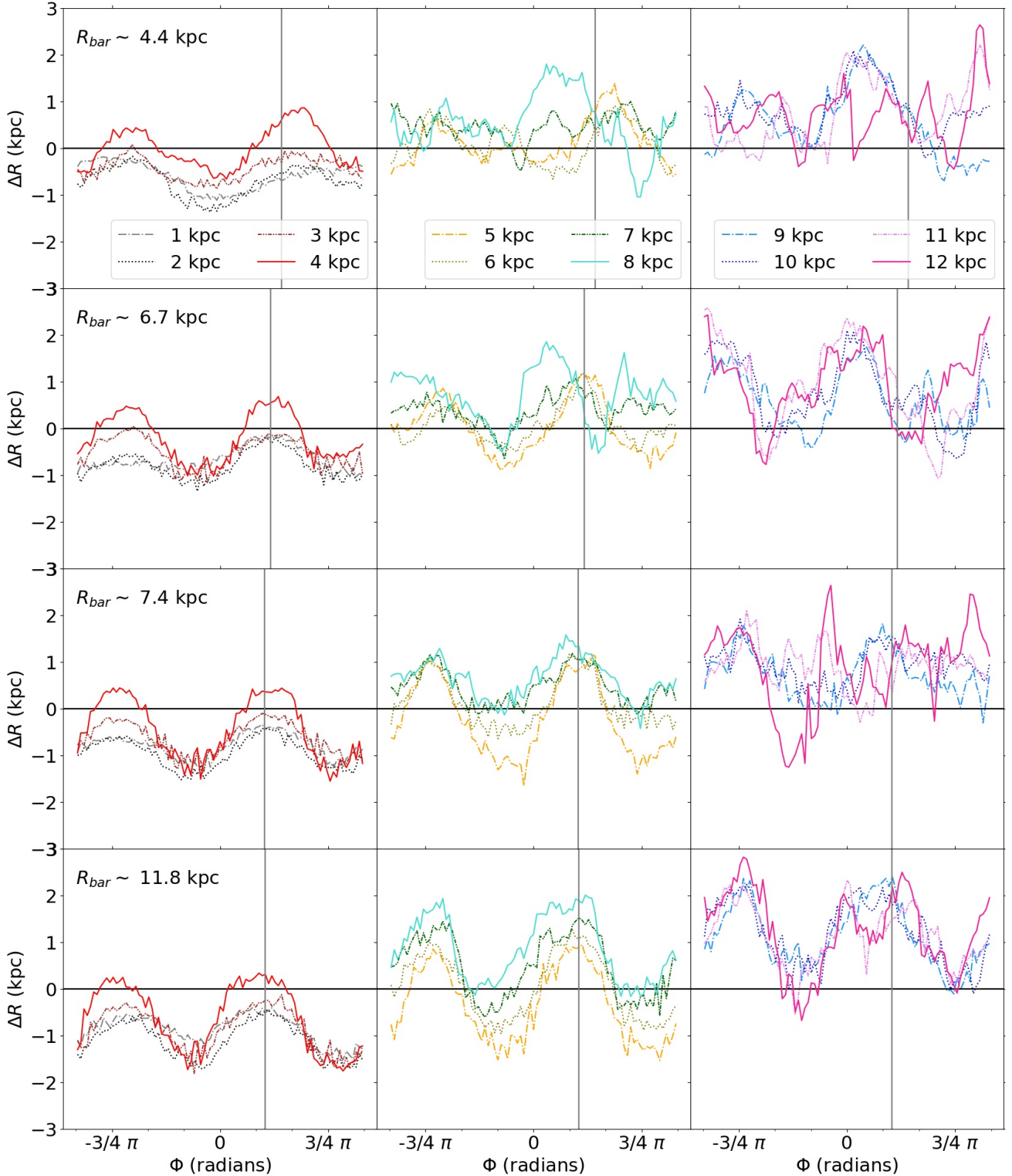


Figure 3. The ΔR (i.e. median distance stars have travelled computed in 4° bins) of stars in each of the twelve annuli as a function of angle at the four time intervals considered in this analysis (rows correspond to $\Delta t = 1, 2, 3, 4$ Gyr from top to bottom). Vertical grey line indicates the angle of the bar at that time. Left column: the four innermost annuli, centered on 1 through 4 kpc. Middle column: the four middle annuli, centered on 5 through 8 kpc. Right column: the four outermost annuli, centered on 9 through 12 kpc. The center of each annulus is indicated with the colour and line style pairing given in the legend. The three innermost annuli (left column) are entirely below the x-axis at all times, indicating that orbits that have evolved inward in these annuli. The four outermost annuli (right column) are predominantly above the x-axis, indicating that orbits that have evolved outward in these annuli. The trends in the six outermost annuli (middle and right column) become more sinusoidal and aligned with the bar angle at later times (lower rows).

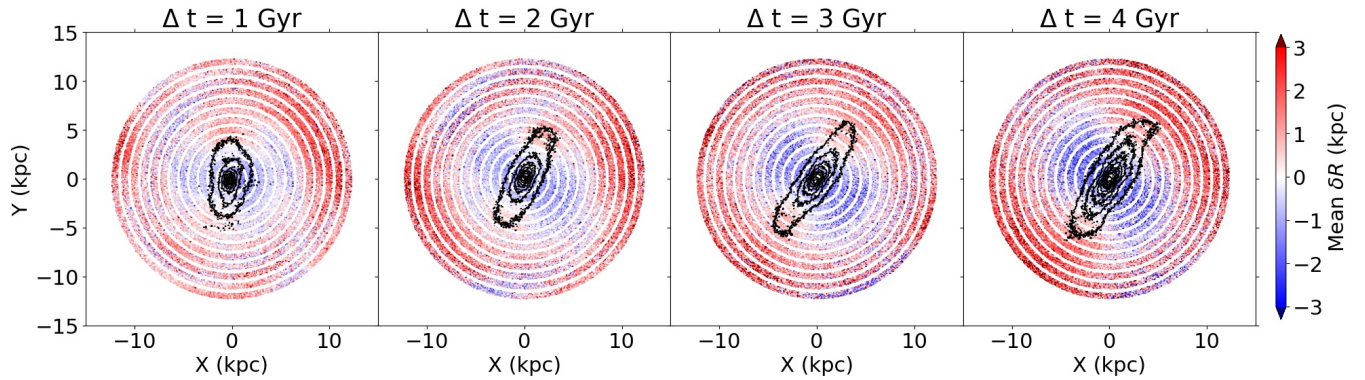


Figure 4. Two-dimensional histograms in X and Y of the twelve annuli at each time, colour-coded by the mean δR in each ~ 0.1 kpc-wide hexagonal bin. Over-plotted in black are isodensity contours of the stellar disc, which rotates counter-clockwise.

Table 1. The maximum and minimum values of ΔR and the angle-averaged δR in each annulus at each time interval.

	Maximum ΔR (kpc)				Minimum ΔR (kpc)				$\langle \delta R \rangle_\phi$ (kpc)			
	1 Gyr	2 Gyr	3 Gyr	4 Gyr	1 Gyr	2 Gyr	3 Gyr	4 Gyr	1 Gyr	2 Gyr	3 Gyr	4 Gyr
Annulus 1	-0.19	-0.16	-0.34	-0.41	-1.12	-1.11	-1.37	-1.52	-0.76	-0.87	-1.04	-1.10
Annulus 2	-0.18	-0.19	-0.42	-0.45	-1.37	-1.35	-1.52	-1.72	-0.67	-0.75	-0.91	-1.10
Annulus 3	0.06	0.04	-0.10	-0.13	-0.87	-1.18	-1.35	-1.81	-0.36	-0.37	-0.48	-0.75
Annulus 4	0.86	0.68	0.44	0.33	-0.66	-1.02	-1.56	-1.76	0.02	-0.05	-0.08	-0.26
Annulus 5	1.38	1.17	1.15	0.95	-0.60	-0.90	-1.65	-1.53	0.05	0.11	0.19	0.09
Annulus 6	0.91	1.17	1.16	1.27	-0.66	-0.50	-0.65	-0.97	0.11	0.02	0.29	0.29
Annulus 7	0.99	1.07	1.18	1.52	-0.48	-0.67	-0.13	-0.61	0.37	0.29	0.41	0.57
Annulus 8	1.80	1.85	1.58	2.01	-1.05	-0.54	-0.43	-0.17	0.55	0.64	0.59	0.89
Annulus 9	2.20	1.74	1.82	2.40	-0.70	-0.43	-0.31	-0.11	0.73	0.75	0.83	1.25
Annulus 10	2.08	2.10	1.91	2.23	-0.21	-0.65	0.08	-0.10	0.97	1.03	1.07	1.44
Annulus 11	2.21	2.58	2.11	2.33	-0.33	-1.07	-0.29	-0.54	0.90	1.16	1.05	1.49
Annulus 12	2.64	2.43	2.64	2.82	-0.45	-0.77	-1.26	-0.68	0.87	1.12	1.14	1.46

we are aware and should be ubiquitous in galaxies with bar evolution. As we discuss below, in Section 5.2, these effects must be included in semi-analytic models of disc evolution – simple diffusion does not inherently include these bar-driven effects.

The net inwards evolution in the innermost annuli is characteristic of angular momentum loss due to the secular evolution of the bar (see e.g. Petersen et al. 2019), and thus is a generic result for evolving barred galaxies. The net effect of secular evolution and dynamical response (i.e. reaction to the non-axisymmetric potential) can be most easily seen in the angle-averaged distance that stars have travelled at a given annulus (i.e. $\langle \delta R \rangle_\phi$) in Table 1. The angle-dependent peaks (minimum and maximum ΔR) occur in concert with this net change. This radial rearrangement can be significant: at $\Delta t = 3$ Gyr, for example, stars travelled an angle-averaged radial distance of ~ 1 kpc to enter the annulus centered on 2 kpc. That is, stars in that annulus at $\Delta t = 3$ Gyr started at radii that were, on average, $\sim 2\times$ larger. The average outwards evolution in the outer disc is likely due to the net effect of the bar (and its trailing structure) moving angular momentum outwards, though the radius-dependent decrease in stellar density

probably also contributes to this signal (as suggested by Kubryk et al. 2013).

The disc can thus be thought of as having three radial ‘zones’, and these zones arise due to the combined effect of secular evolution and dynamical response of orbits. The physical radii that these zones occupy will depend on the properties of the bar, and above we provide the approximate radial ranges of these zones in terms of the R_d and R_{bar_0} of this simulation. We can further define these zones more precisely using $\langle \delta R \rangle_\phi$. We illustrate these zones and their evolution in Figure 5, which shows $\langle \delta R \rangle_\phi$ and the minimum and maximum ΔR at each time step alongside the approximate bar length and corotation radii. Here, we define the inner zone to be where $\langle \delta R \rangle_\phi \leq -0.25$, the intermediate zone to be where $-0.25 < \langle \delta R \rangle_\phi < 0.25$, and the outer zone to be where $0.25 \leq \langle \delta R \rangle_\phi$. The inner and intermediate zone are both interior to corotation at each time interval. In the inner zone, where orbits have on average evolved inwards, angle-dependent trends are well-aligned with the bar angle and ΔR and $\langle \delta R \rangle_\phi$ are generally below zero. In the intermediate zone, there is no mean radial evolution and the angle-dependent ΔR trends are

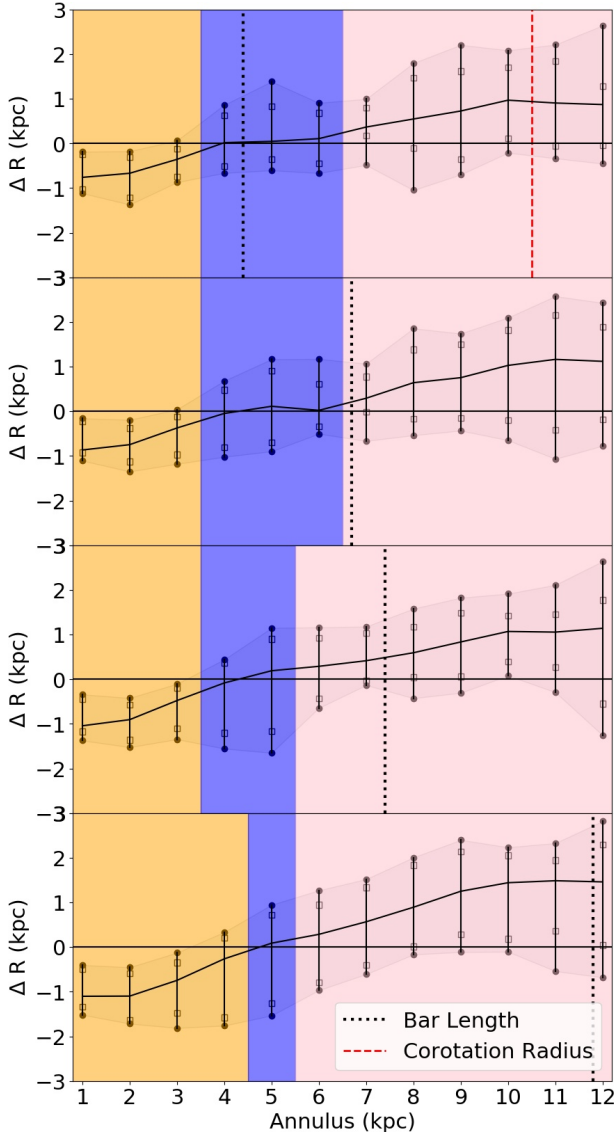


Figure 5. The maximum and minimum ΔR (solid black circles) for stars in each of the twelve annuli at the four time intervals considered in this analysis (rows correspond to $\Delta t = 1, 2, 3, 4$ Gyr from top to bottom) alongside the bar length and approximate corotation radius at that time (black dotted and red dashed lines, respectively, note that at most times corotation is beyond 12 kpc). The tenth and ninetieth quantiles of ΔR are shown as black open squares, and the $\langle \delta R \rangle_\phi$ in each annulus is plotted as the solid black line. The inner zone, defined to be where $\langle \delta R \rangle_\phi \leq -0.25$, is shaded in orange. The intermediate zone, where $-0.25 < \langle \delta R \rangle_\phi < 0.25$, is shaded in blue, and the outer zone, where $0.25 \geq \langle \delta R \rangle_\phi$, is shaded in pink. For reference, R_d and R_{bar_0} are 3 and ~ 4.3 kpc, respectively.

roughly symmetric around zero - i.e. $\langle \delta R \rangle_\phi \sim 0$ kpc. Finally, in the outer zone, orbits generally evolved outwards, $\langle \delta R \rangle_\phi > 0$ kpc, and angle-dependent trends are generally less well-aligned with the bar angle.

3.3 Comparison to Pre-Bar Formation Initial Radii

For completeness, we compare our results to those that would be obtained if we instead defined the initial radii to correspond to a time prior to bar formation. We repeat the procedure above, but adopt an initial time of $t = 0$ ($\Delta t \sim -2.2$ Gyr in Figure 1), when there is no

structure in the disc. In comparison to the results seen in Figure 3, we find that the shape and phase of the ϕ versus ΔR curves remain largely unchanged, but the annuli centered on radii larger than $\sim R_d$ are generally shifted towards higher $\langle \delta R \rangle_\phi$ and more positive ΔR values. The radial locations and extents of each of the zones changes accordingly. For example, at 2 Gyr post bar-formation, the annulus centered on 6 kpc has $\langle \delta R \rangle_\phi \sim 0.5$ kpc if the initial radii of stars is defined at $t = 0$, compared to ~ 0.0 kpc if the initial radii are defined at $t = t_0$. The general shift outward is likely the same disc expansion mentioned in Di Matteo et al. (2013), and is a sign of the angular momentum re-arrangement that must occur in the disc during bar formation.

This exercise also allows us to test the sensitivity of our results to two of our assumptions about how stars are ‘born’ in galaxies. First, in defining the initial radial locations of stars to correspond to a time after the bar formed, we effectively assumed that the density distribution of newly ‘born’ stars matches that of the older stars at $t = t_0$. Second, we did not require that stars originate on circular orbits at $t = t_0$. Star formation in barred galaxies in nature may differ from this extreme, but comparison to the opposite extreme (i.e. the smooth disc at $t_0 = 0$) indicates that our results are largely insensitive to – and so robust against – variations in these assumptions. The main difference in the bulk radial changes that occur in these two extremes is that there is additional exchange of angular momentum in the case of the smooth disc, which is an anticipated effect of the bar formation process.

4 A TOY MODEL

One of the fundamental difficulties in relating dynamical analyses of pure N-body simulations to nature is the fact that initial (birth) radii of stars are not directly observable quantities. This problem is frequently circumvented by assuming that stars form following some kind of initial metallicity gradient, such that the metallicity of stars can be used as an observational tracer of their birth radius. We here assume that stars in the Milky Way are born with metallicities that generally follow a radius-dependent gradient, and we employ a simple toy model with metallicities ‘painted’ on to the stars in our N-body simulation. This toy model, though an over-simplification, allows us to explore the potential signatures and trends of the bulk radial changes in metallicity space.

In our toy model, we assign metallicities to stars as a function of their (cylindrical, galactocentric) initial radius in our simulation, following the functional form in Di Matteo et al. (2013):

$$Z(R) = Z_0 10^{\gamma R_0} \quad (2)$$

where Z_0 is three times the solar value, R_0 is the initial (‘birth’) radius at $t = t_0$, and γ is the metallicity gradient. We set $\gamma = -0.07$ dex per kpc (generally matching present-day observations of younger red giant branch stars, see e.g. Anders et al. 2017). We adopt $\frac{Z_\odot}{X_\odot} = 0.0207$ (consistent with the PARSEC stellar evolutionary tracks, Bressan et al. 2012), such that the metallicity at the center of the galaxy is $[\text{M}/\text{H}] \sim 0.5$. As we are assuming that all stars have the same age, the resulting metallicity trends would be most readily comparable to those in a mono-age population across the disc.

The amplitude of the angle-dependent ΔR variations are dependent on the strength of the non-axisymmetric perturbation (e.g. the bar), while variations in metallicity space will have an additional dependence on the slope of the initial metallicity gradient (Di Matteo et al. 2013). We note that our results are not strongly dependent on the slope or functional form of the initial gradient – as long as there

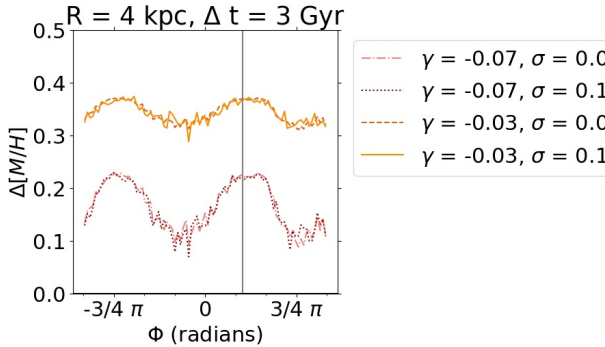


Figure 6. The angle-dependent median metallicity variations ($\Delta[M/H]$) in the annulus centered on 4 kpc at $\Delta t = 3$ Gyr if different metallicity gradients ($\gamma = -0.07$ in red, $\gamma = -0.03$ in orange) and dispersions (line styles indicated in legend) are adopted.

is some type of measurable radius-dependent initial gradient, there should exist a mapping between ΔR and metallicity variations. We illustrate this in Figure 6, which shows the angle-dependent median metallicity variations ($\Delta[M/H]$, the median metallicity value of the stars within the same 4° azimuth bins used in Section 2.3) if different values of the gradient (γ) and dispersion (σ) are adopted. We incorporate metallicity dispersion by adding to the metallicity of each star a random value drawn from a Gaussian distribution centered on zero with width σ . For clarity, only the metallicity variations in the annulus centered on 4 kpc at $\Delta t = 3$ Gyr are shown.

In this toy model, the radial rearrangement occurring in the disc results in angle-dependent variations in the median metallicity at a given annulus. Metal-rich regions in an annulus (i.e. peaks in ΔR) are aligned with the angle of the bar out to approximately R_{bar} , and are increasingly less well-aligned at larger radii (in agreement with Di Matteo et al. 2013). The inner zone, where orbits have evolved inwards, is more metal-poor on average than its initial metallicity (at $t = t_0$), while the outer zone, where orbits have evolved outwards, is more metal-rich.

4.0.1 Caveats

The presence of a present-day radial metallicity gradient for stars of a given age does not necessarily imply that those stars were born with a metallicity distribution that followed that gradient. Indeed, as discussed in Schönrich & McMillan (2017), the present-day radial gradient is determined by the gradient of the star-forming interstellar medium, the spatial dependence of star formation, and the radial rearrangement of stars in the disc. It is also likely that a Galactic bar would impact star formation and gas enrichment, and these effects may not be fully captured with a smooth radius-dependent initial metallicity gradient. It is perhaps for these reasons that sinusoidal angle-dependent metallicity variations, while common, are not necessarily ubiquitous in barred simulations (for example, the N-body smoothed particle hydrodynamics simulation presented in Kubryk et al. 2013 has angle-dependent metallicity variations dissimilar to those discussed here, see their Figure 13). The N-body simulation that we use for this analysis lacks gas, star formation, and chemical evolution, and thus this discussion is necessarily over-simplified. We leave further investigation of these important effects to future works.

It is prudent to investigate alternative, metallicity-independent tracers, especially given the uncertainties described above and the need for an observable quantity to link dynamical analyses (such as this one) to nature. For example, it may be possible to identify bulk

radial changes in the disc via stellar age distributions if the galaxy had a radius-dependent star formation history.

4.1 Observational Signatures in the Milky Way

Our model, while simplistic, allows us to consider how dynamics may be connected to observable trends. Recent analyses have revealed hints of angle-dependent stellar metallicity variations in the Milky Way disc (Gaia Collaboration et al. 2022, Poggio et al. 2022, Hawkins 2022). The amplitude and morphology of these azimuthal variations is dependent on the tracer stellar population. Samples of giant stars show azimuthal metallicity variations at the level of ~ 0.1 dex, with the metal-rich regions aligned with the known spiral arm over-densities (Hawkins 2022, see also Poggio et al. 2022). However, this pattern is dependent on the effective temperature (and thus age) of the tracer population: Poggio et al. (2022) find that the alignment of metallicity variations with the spiral over-densities is seen most strongly in the hottest young stars ($\lesssim 100 - 300$ Myr) and is nearly non-existent in the cooler, relatively older, stars.

Indeed, kinematically cooler (i.e. younger) components are predicted to react more strongly to perturbations than kinematically hotter (i.e. older) components (e.g. Solway et al. 2012, Vera-Ciro et al. 2014, Vera-Ciro et al. 2016, Daniel & Wyse 2018). In discs with *vertical* initial metallicity gradients, this differential response can cause azimuthal metallicity variations (Khoperskov et al. 2018). However, given the very young ages of the hottest stars, the observed azimuthal variations in this population may be more indicative of recent star formation and enrichment trends.

Other stellar tracers have azimuthal metallicity variations of similar amplitude that do not appear to be aligned with spiral structure. The sample of OB stars shown in Hawkins (2022) and some samples of giant stars (dependent on the properties of the sample, see the ‘RGB’ sample in Gaia Collaboration et al. 2022 and the cooler giant sample in Poggio et al. 2022) have metallicity distributions that are asymmetric in the X-Y plane, with more metal-rich stars ahead of the Sun. Gaia Collaboration et al. (2022) note that it is plausible that this concentration of metal-rich stars could be aligned with the bar, which generally matches the trends predicted by our simple toy model. Those authors further find that their RGB sample has lower metallicity than what would be predicted by a smooth radius-dependent initial metallicity gradient in the inner disc, as is also predicted by our toy model. However, for the reasons given above, the utility of our toy model in these comparisons is limited. Additional analyses of the observational data (particularly those employing a larger range of ϕ angles and incorporating age information) and further simulations are required to investigate the plausible origins of these observed trends.

4.2 Transforming Metallicity Information into Information on Bulk Radial Changes

There have been a number of analyses in the literature that aim to determine birth radii of individual stars in the Milky Way (see e.g. Minchev et al. 2018, Feltzing et al. 2020, Lu et al. 2022a). These analyses generally estimate the age for a given star and identify its likely birth radius by comparing its metallicity to a model of the initial metallicity distribution in the disc at the time of the star’s birth. A similar analysis could be done to constrain the *bulk* radial changes that occurred in the disc. Indeed, as initial metallicity gradients are inherently information about *average* (or median) trends, we argue that it is more appropriate to use such a procedure to estimate the

trends and amplitude of bulk radial changes than to determine birth radii for individual stars. Further, dispersion in the initial metallicity distribution could cause there to be significant uncertainties for individual birth radii (see e.g. Lu et al. 2022b), but it should have minimal impact on the measured mean or median metallicity for a given radius and azimuthal bin (see Figure 6).

4.2.1 Learning About the Initial Gradient

If there are multiple episodes of star formation after the bar formed, the bulk radial re-arrangement trends in a given annulus should be broadly similar in each of the resulting populations after a few orbital periods. The differential response of cooler and hotter components (as discussed above, e.g. Khoperskov et al. 2018) could cause the amplitude of the ΔR (or metallicity) signal to differ between populations of different ages, but should not affect the over-all behavior of stars in the three zones in the disc. It may be possible to use this idea to constrain the time evolution of the initial metallicity gradient. For example, one could divide the stars in the disc into different age bins and then estimate the ΔR from the median metallicity information, as outlined above, with some assumed model for the initial metallicity gradient. Large disagreement in resulting bulk trends from different age bins at the same annulus could indicate that the adopted model of the initial metallicity gradient is inappropriate. It could further be required that the innermost annuli exhibit net inwards evolution (i.e. negative ΔR) if it is known that the bar is evolving.

The feasibility of providing such constraints in nature depends on the details of how star formation and chemical enrichment are carried out in barred galaxies, as well as how accretion of both stars and gas over time alter the chemical composition and gravitational potential. Additional investigations with chemo-dynamical (and possibly extremely high resolution cosmological) simulations are required to further test the predictions given here, which we leave to future studies.

4.3 Future Prospects

Spectroscopic observations focused on younger-to-intermediate age stars that cover a wide range of ϕ angles in the inner ~ 5 kpc of the Milky Way would be optimal for detecting bar-driven trends such as those predicted by our toy model. Younger stars should have experienced fewer total large-scale changes to the galactic potential compared to older stars that will have experienced the formation of the bar and potentially the most recent major merger (i.e. *Gaia* Sausage-Enceladus, Belokurov et al. 2018, Helmi et al. 2018, which would both infuse fresh gas for star formation and change orbits via altering the gravitational potential). The observed stars should be young enough to have been born after the bar formed, but old enough to have completed a few orbits. Beyond defining the sample, age estimates would be critical to the analysis as the mapping between ΔR and metallicity is most accurate for stars of approximately the same age.

Compared to the Solar neighborhood, observations in the inner disc can more easily obtain the ϕ coverage needed to characterise any angle-dependent metallicity variations: mapping just a quarter of the predicted sinusoidal ϕ versus metallicity curve requires a ϕ coverage of $\sim 90^\circ$. The inner disc is also where the bar-driven, angle-dependent ΔR (and thus metallicity) trends should be most coherent and aligned with the bar (see above, also note the Milky Way has a bar length of ~ 5 kpc, Wegg et al. 2015). The currently available spectroscopic data are rather patchy in the interior regions of the Galaxy, but the

upcoming SDSS-V, 4MOST, and MOONS spectroscopic surveys will each map the inner disc (see e.g. Kollmeier et al. 2017, Chiappini et al. 2019, Gonzalez et al. 2020) and provide relevant data.

Looking beyond the Milky Way, we note that it may soon be possible to detect azimuth angle-dependent metallicity variations in the resolved stellar populations of M31 using spectra of individual red giant branch stars. Given the known non-axisymmetric features (e.g. a bar, Athanassoula & Beaton 2006) it is likely that M31 is host to azimuth angle-dependent trends in ΔR , which may or may not be similar to those in the Milky Way. Indeed, studies using photometric metallicities have indicated that there may be a metal-rich region aligned with the bar (Gregersen et al. 2015). The first wide-field, massively multiplexed spectroscopic surveys that are capable of measuring metallicities of individual red giant stars in M31 are coming online, such as PFS and DESI (see e.g. Takada et al. 2014, Dey et al. 2022), which can provide the data to enable more detailed exploration of azimuthal metallicity variations in the disc of M31.

5 DISCUSSION

The ΔR and $\langle \delta R \rangle_\phi$ trends discussed in this analysis have revealed that the response of the disc to a bar is both radius- and azimuth angle-dependent. Further, the effects of dynamic response and secular evolution are coupled. While we compute ΔR and $\langle \delta R \rangle_\phi$ with t_0 defined to be post bar-formation, the results highlighted here remain true even if the initial time instead corresponds to the start of the simulation ($t = 0$), before structure forms. The main difference between these two scenarios is that when $t = 0$, there is additional angular momentum transfer associated with the formation of the bar that causes ΔR and $\langle \delta R \rangle_\phi$ to tend towards higher positive values (increase in radius). The three radial zones shift accordingly.

The bulk trends in the inner disc, i.e. inwards evolution in concert with angle-dependent trends that are aligned with the bar, indicate that stars can experience both an increase in eccentricity and a change in angular momentum (see also Ghosh et al. 2022 for further discussion). One can see how this naturally arises within the region most strongly dominated by the bar. Here, the ϕ location of the (radial) apses of stars tend to align with the bar major axis. As orbits become more eccentric, they create peaks of ΔR that are then aligned with the bar major axis, while troughs will be aligned with the minor axis. These peaks and troughs occur in addition to whatever bulk exchange of angular momentum occurs. Analyses that focus solely on stars that change angular momentum but do not become eccentric, and vice-versa, thus paint an incomplete picture of the evolution within the disc. Similarly, analyses focusing only on the angle-dependent trends may miss the broader radius-dependent evolution in the disc. Below, we comment on two additional implications of our results.

5.1 Morphology of Bulk Radial Changes in Context

Galactic bars are not the only possible source of angle-dependent ΔR variations – spiral arms and the gravitational perturbations from a merging satellite could also cause such signals. As discussed above, bar-driven, angle-dependent ΔR variations will be aligned with the bar within the bar-dominated region and will start to be offset from the bar angle at radii larger than the bar length, where trailing structure begins. Indeed, the degree of alignment of ΔR variations with the bar angle could help discern where the transition between bar and trailing structure occurs. Spiral-driven angle-dependent ΔR variations will align with the spiral (see e.g. metallicity variations in Khoperskov

et al. 2018) such the phase of the ϕ versus ΔR curve will vary as a function of radius.

The ΔR variations induced by an orbiting satellite need not align with any internal structure, and should be strongest near the location of the pericenter passage. Carr et al. (2022) show for a Milky Way-like galaxy experiencing a Sagittarius-like merger, the variations of the change of angular momentum and metallicity in the X-Y plane will look somewhat like a quadrupole but will not necessarily be symmetric in distribution or strength. The differing behavior of the ϕ -dependent trends as a function of radius resulting from these three different origins provide hope that it may be possible to disentangle the cause of observed angle-dependent trends if given sufficient spatial information. In particular, in the outer disc within a limited spatial range the three signals discussed here may appear quite similar. As such, special care should be taken in interpreting the origins of any ϕ versus ΔR trends at large R .

5.2 Implications for Semi-Analytic Modelling

The results presented here should be included in future semi-analytic modelling analyses of the radial evolution of orbits (see e.g. Schönrich & Binney 2009, Brunetti et al. 2011, Frankel et al. 2018 for recent examples of such analyses). Such analyses typically model the radial changes of stars in the disc as a diffusion process with some dependence on age. However, a diffusion process alone does not describe the bulk radial changes driven by a galactic bar. As shown in this analysis, it is crucial to include a radial and azimuthal dependence on the distance that stars travel within the disc of a barred galaxy. Angle-dependence in semi-analytic modelling is likely also important for spiral galaxies with weak or non-existent bars (see e.g. Grand et al. 2016, Khoperskov et al. 2018).

6 CONCLUSION

We investigate the radial re-distribution of stars that occurs in an N-body simulation of a disc galaxy after a bar has formed. We summarise the conclusions of this analysis as follows:

- The bar induces azimuth angle-dependent and radius-dependent trends in the median distance that stars have travelled to enter a given annulus. The azimuthal trends are aligned with the bar out to approximately the end of the bar and become offset at larger radii. Angle dependent trends are present throughout the disc.
- The radius-dependent trends divide the disc into three zones. On average, stars currently in the inner zone (where $\langle \delta R \rangle_\phi$ is less than zero, here $R \lesssim R_d$, $R \lesssim R_{\text{bar}_0}$) originated at larger radii and their orbits have evolved inwards. Stars currently in the intermediate zone (where $\langle \delta R \rangle_\phi$ is near zero, here $R \gtrsim R_d$, $R \gtrsim R_{\text{bar}_0}$) could have originated at larger or smaller radii, and there is no net radial evolution (i.e. ΔR is roughly symmetric about zero). Finally, stars in the outer zone (where $\langle \delta R \rangle_\phi$ is greater than zero, here $R > R_{\text{bar}_0}$) on average originated at smaller radii and their orbits evolved outwards.
- We assign metallicities to the star particles in our simulation following a radial metallicity gradient and explore the metallicity trends in this toy model. The radial re-arrangement in the disc causes the inner and outer zones become more metal-poor and metal-rich, respectively, than their initial metallicities. Peaks of ΔR in a given annulus correspond to metal-rich regions in this model.
- We discuss recent observational evidence for angle-dependent metallicity variations in the Milky Way, and find that some of these trends are plausibly related to the bar-driven trends predicted here.

We comment on the possibility of using observed angle-dependent median metallicity trends to learn about the initial metallicity gradient and the bulk radial changes that have occurred in the disc.

Future analyses of the angle- and radius-dependent trends in barred galaxies are necessary to further explore the ideas presented here. For example, it would be prudent to test the predictions given in Section 4 with simulations of barred galaxies that include gas, star formation, and galactic mergers. Observation-based analyses also hold exciting promise as new spectroscopic surveys enable wider and more dense coverage of the Milky Way disc and beyond.

DATA AVAILABILITY

The simulation used in this analysis will be made available upon reasonable request. The following codes were used in the analysis and production of this manuscript: EXP (Weinberg 1999; Petersen et al. 2022), Matplotlib (Hunter 2007), numpy (Harris et al. 2020), pandas (Wes McKinney 2010), and scipy (Virtanen et al. 2020).

7 ACKNOWLEDGMENTS

The authors thank the Flatiron Institute’s Center for Computational Astrophysics and the Big Apple Dynamics school for making this work possible. CF would like to thank Keith Hawkins, Chris Carr, Mike Petersen, Jason Hunt, and Rosemary F.G. Wyse for insightful conversation. CF acknowledges support by the NASA FINESST grant and support through the generosity of Eric and Wendy Schmidt, by recommendation of the Schmidt Futures program. Contributions by RLM to this material are supported by the Wisconsin Space Grant Consortium under NASA Award No. 80NSSC20M0123, the Ruth Dickie Endowment of the UW-Madison Beta Chapter of SDE/GWIS, and the National Science Foundation Graduate Research Fellowship under Grant No. 2137424. KJD gratefully acknowledges the Flatiron Institute’s Center for Computational Astrophysics for hosting her during the course of this work.

REFERENCES

Anders F., et al., 2017, *A&A*, **600**, A70
 Athanassoula E., Beaton R. L., 2006, *MNRAS*, **370**, 1499
 Athanassoula E., Misiriotis A., 2002, *MNRAS*, **330**, 35
 Baba J., Kawata D., Schönrich R., 2022, *MNRAS*, **513**, 2850
 Belokurov V., Erkal D., Evans N. W., Koposov S. E., Deason A. J., 2018, *MNRAS*, **478**, 611
 Binney J., Tremaine S., 2008, *Galactic Dynamics: Second Edition*. Princeton University Press
 Blitz L., Spergel D. N., 1991, *ApJ*, **379**, 631
 Bressan A., Marigo P., Girardi L., Salasnich B., Dal Cero C., Rubele S., Nanni A., 2012, *MNRAS*, **427**, 127
 Brunetti M., Chiappini C., Pfenniger D., 2011, *A&A*, **534**, A75
 Carr C., Johnston K. V., Laporte C. F. P., Ness M. K., 2022, *MNRAS*, **516**, 5067
 Chiappini C., et al., 2019, *The Messenger*, **175**, 30
 D’Onghia E., L. Aguerri J. A., 2020, *ApJ*, **890**, 117
 Daniel K. J., Wyse R. F. G., 2018, *MNRAS*, **476**, 1561
 Dey A., et al., 2022, arXiv e-prints, p. arXiv:2208.11683
 Di Matteo P., Haywood M., Combes F., Semelin B., Snaith O. N., 2013, *A&A*, **553**, A102
 Feltzing S., Bowers J. B., Agertz O., 2020, *MNRAS*, **493**, 1419
 Fragkoudi F., Di Matteo P., Haywood M., Schultheis M., Khoperskov S., Gómez A., Combes F., 2018, *A&A*, **616**, A180

Frankel N., Rix H.-W., Ting Y.-S., Ness M., Hogg D. W., 2018, [ApJ, 865, 96](#)
 Gaia Collaboration et al., 2022, arXiv e-prints, [p. arXiv:2206.05534](#)
 Ghosh S., Fragkoudi F., Di Matteo P., Saha K., 2022, arXiv e-prints, [p. arXiv:2210.14244](#)
 Gonzalez O. A., et al., 2020, [The Messenger, 180, 18](#)
 Grand R. J. J., et al., 2016, [MNRAS, 460, L94](#)
 Gregersen D., et al., 2015, [AJ, 150, 189](#)
 Harris C. R., et al., 2020, [Nature, 585, 357](#)
 Hawkins K., 2022, arXiv e-prints, [p. arXiv:2207.04542](#)
 Helmi A., Babusiaux C., Koppelman H. H., Massari D., Veljanoski J., Brown A. G. A., 2018, [Nature, 563, 85](#)
 Hunter J. D., 2007, [Computing in Science & Engineering, 9, 90](#)
 Hwang H.-C., et al., 2019, [ApJ, 872, 144](#)
 Khoperskov S., Di Matteo P., Haywood M., Combes F., 2018, [A&A, 611, L2](#)
 Kollmeier J. A., et al., 2017, arXiv e-prints, [p. arXiv:1711.03234](#)
 Kubryk M., Prantzos N., Athanassoula E., 2013, [MNRAS, 436, 1479](#)
 Lu Y., Minchev I., Buck T., Khoperskov S., Steinmetz M., Libeskind N., Cescutti G., Freeman K. C., 2022a, arXiv e-prints, [p. arXiv:2212.04515](#)
 Lu Y., Buck T., Minchev I., Ness M. K., 2022b, [MNRAS, 515, L34](#)
 Lynden-Bell D., Kalnajs A. J., 1972, [MNRAS, 157, 1](#)
 Minchev I., et al., 2018, [MNRAS, 481, 1645](#)
 Navarro J. F., Frenk C. S., White S. D. M., 1997, [ApJ, 490, 493](#)
 Petersen M. S., Weinberg M. D., Katz N., 2019, [MNRAS, 490, 3616](#)
 Petersen M. S., Weinberg M. D., Katz N., 2021, [MNRAS, 500, 838](#)
 Petersen M. S., Weinberg M. D., Katz N., 2022, [MNRAS, 510, 6201](#)
 Poggio E., et al., 2022, [A&A, 666, L4](#)
 Schönrich R., Binney J., 2009, [MNRAS, 396, 203](#)
 Schönrich R., McMillan P. J., 2017, [MNRAS, 467, 1154](#)
 Sellwood J. A., Athanassoula E., 1986, [MNRAS, 221, 195](#)
 Solway M., Sellwood J. A., Schönrich R., 2012, [MNRAS, 422, 1363](#)
 Takada M., et al., 2014, [PASJ, 66, R1](#)
 Vera-Ciro C., D'Onghia E., Navarro J., Abadi M., 2014, [ApJ, 794, 173](#)
 Vera-Ciro C., D'Onghia E., Navarro J. F., 2016, [ApJ, 833, 42](#)
 Virtanen P., et al., 2020, [Nature Methods, 17, 261](#)
 Wegg C., Gerhard O., Portail M., 2015, [MNRAS, 450, 4050](#)
 Weinberg M. D., 1992, [ApJ, 384, 81](#)
 Weinberg M. D., 1999, [AJ, 117, 629](#)
 Wes McKinney 2010, in Stéfan van der Walt Jarrod Millman eds, Proceedings of the 9th Python in Science Conference. pp 56 – 61, [doi:10.25080/Majora-92bf1922-00a](#)
 Wheeler A., Abril-Cabezas I., Trick W. H., Fragkoudi F., Ness M., 2022, [ApJ, 935, 28](#)